SUPPLEMENTAL MATERIALS for

THz vortex beam as a spectroscopic probe of magnetic excitations

A. A. Sirenko[1]*, P. Marsik[2], C. Bernhard[2], T. N. Stanislavchuk[1], V. Kiryukhin[3], and S-W. Cheong[3]

[1] Department of Physics, New Jersey Institute of Technology, Newark, New Jersey 07102, USA

[2] Department of Physics, University of Fribourg, CH-1700 Fribourg, Switzerland

[3] Rutgers Center for Emergent Materials and Department of Physics and Astronomy, Rutgers University, Piscataway, New Jersey 08854, USA

* Correspondence and requests for materials should be addressed to A. A. S. (email: sirenko@njit.edu)

1. Structural properties of the $Dy_3Fe_5O_{12}$

$Dy_3Fe_5O_{12}$ belongs to the family of rare-earth (R) iron garnets (R-IG) [1,2]. At room temperature, $Dy_3Fe_5O_{12}$ crystals form a cubic structure with 8 formula units and a space group $Ia3d$(O_h^{10}). The Fe^{3+} ions occupy 16a octahedral sites with $\bar{3}$ (C_{3i}) symmetry and 24c tetrahedral sites with $\bar{4}$ (S_4) symmetry. Dy^{3+} ions with the ground state ${}^6H_{15/2}$ are in 24d dodecahedral sites with the local orthorhombic symmetry 222(D_2). There are several non-equivalent Dy^{3+} ions in each unit cell with the same surrounding field, but their axes are inclined to each other. This has the overall effect of producing an average quasi-cubic symmetry. The main magnetic superexchange interaction is between Fe in two different sites (a and c). Below T_N the spins of Fe in the tetrahedral site are antiparallel to those of the octahedral site forming a *ferri*magnetic structure along the [1 1 1] direction [1,2]. Furthermore, the Dy moments are antiparallel coupled to the Fe moments in the tetrahedral site and thus to the net ferrimagnetic moment of the whole Fe sublattice. Below 100 K, a rhombohedral distortion of the cubic cell causes a canting of the Dy spins, which is described as a "double umbrella structure" [3] The symmetry of Dy^{3+} is lowered from 222(D_2) tetragonal to 2(C_2) monoclinic. Below 50 K, the iron sublattice magnetization does not change appreciably with temperature. However, the Dy sublattice magnetization increases rapidly with the temperature decrease and magnetic ordering of Dy^{3+} appears below T_C=16 K.

2. Low-frequency magnetic excitations in $Dy_3Fe_5O_{12}$

Low-frequency IR-active excitations, such as phonons, ligand field (LF), crystal field (CF), and Kaplan-Kittel (KK) modes were studied previously in Dy-IG [4,5] and in related Tb-IG [6]. The temperature and magnetic field dependencies for the low frequency excitations were analyzed in detail for all but one of the lowest energy frequencies at ~13 cm^{-1}. In this paper, we used two complementary experimental techniques of THz ellipsometry and THz transmission for the polarization analysis of the low-frequency optical excitations in Dy-IG. In our previous studies of the low-frequency spectra of Dy-IG[4,5] we identified several LF and KK excitations of Dy^{3+} with energies at T=5 K of 13 cm^{-1}, 17 cm^{-1}, 23 cm^{-1}, 28 cm^{-1}, 44 cm^{-1}, 51 cm^{-1}, 59.5 cm^{-1}, and the lowest frequency optical phonon at 81 cm^{-1}. Their temperature dependencies from Ref. [4] are reproduced in FIG. 3 of the paper for comparison with the new experimental data. The 23 and 28 cm^{-1} absorption lines, as first proposed by Sievers and Tinkham [7] have pronounced temperature dependencies that are typical for LF transitions with

$$\Omega_{\mathrm{LF}}(T) = g_{\mathrm{Dy}}\mu_{\mathrm{B}}\left[\lambda_{\text{Fe-Dy}}M_{\mathrm{Fe}} + \lambda_{\text{Dy-Dy}}M_{\mathrm{Dy}}(T)\right], \qquad (1)$$

where g_{Dy} is the Dy^{3+} ion g-factor, μ_{B} is the Bohr magneton, M_{Fe} and $M_{\mathrm{Dy}}(T)$ are magnetizations of the corresponding ions, and $\lambda_{\text{Fe-Dy}}$ and $\lambda_{\text{Dy-Dy}}$ are the corresponding exchange interaction constants. The so-called Kaplan-Kittel (KK) modes at 44 cm^{-1} and 51 cm^{-1} have a reversed temperature dependence that corresponds to the mutual precession of Fe spins in the exchange field of Dy^{3+} spins and vice versa [8]:

$$\Omega_{\mathrm{KK}}(T) = \lambda_{\text{Fe-Dy}}\mu_{\mathrm{B}}\left[g_{\mathrm{Dy}}M_{\mathrm{Fe}} - g_{Fe}M_{\mathrm{Dy}}(T)\right]. \qquad (2)$$

The corresponding exchange constants $\lambda_{\text{Fe-Dy}}$ and $\lambda_{\text{Dy-Dy}}$ and g-factors for Dy-IG were determined and summarized in Ref. 4. Temperature dependencies of the LF and KK excitations are similar to those of antiferromagnetic (AFM) resonances, or magnons at $\vec{k} = 0$, in the magnetically-ordered system with several interacting spins. Above the transition temperature T_C=16 K, $M_{\mathrm{Dy}}(T)$ decreases to zero and the corresponding modes with energy $\Omega_{\mathrm{LF}}(T)$ and $\Omega_{\mathrm{KK}}(T)$ behave as temperature-independent crystal field (CF) transitions. The oscillator strength of these modes decreases with temperature and they disappear at $T > 60$ K due to the thermal population of the CF levels. Note here that the difference between LF, KK, and CF modes is not qualitative. The notation of these modes reflects the number of interacting spins involved in their description. Disappearance of the Dy-Fe exchange interaction, which is turned down above T_C, results in a smooth transition between the energies of LF and KK modes to the single ion energies labeled as CF. The detailed description of the collective dispersive nature of the low-temperature modes that include interacting spins of Dy and Fe in two- and three-sublattice models can be found in Ref. 9.

Using a combination of RAE and transmission spectroscopies [4,5,10], it was experimentally confirmed that, as expected, the phonon at 81 cm^{-1} in Dy-IG has a pure electric dipole activity, while most of the Dy^{3+} LF and KK modes have a combined ("hybrid") electric and magnetic dipole activity. The magnetic and electric-dipole oscillator strengths, S_m and S_e, for those modes were experimentally determined. An interesting effect of the adjusted oscillator (AOS) strength for the hybrid modes, which is equal to $S_T \cong \mu_\infty S_e + \varepsilon_\infty S_m$ for transmission geometry and $S_R \cong \mu_\infty S_e - \varepsilon_\infty S_m$ in reflection configuration, was observed [5]. For several modes above 60 cm^{-1}, the AOS effect resulted in an almost perfect cancellation of the mode in reflection, while in transmission measurements such modes were quite strong. Thus, the aforementioned experiments [4,5,10] for phonons, LF, and KK transitions of Dy^{3+} provide a detailed roadmap for the new spectroscopic studies of Dy-IG using vortex beams. Furthermore, the interacting spins of Dy and Fe in two non-equivalent positions, make this magnetically-ordered ferrimagnetic system attractive for spectroscopy of collective magnetic excitation, such as LF and KK modes, using vortex beams.

3. Application of axicons for generation of the vortex beams

Fig. 1 of the manuscript shows a linearly polarized THz beam (from the right) slowly focused towards the sample (on the left). The linear polarization of the THz radiation $(\vec{e}_x \pm \vec{e}_y)$ is controlled by a wire grid linear polarizer with an extinction ratio of 1:200. After the linear polarizer, the light passes through a stationary 2-bounce Fresnel prism retarder. The light beam becomes circularly

polarized $\vec{e}_R$ or $\vec{e}_L$ depending on the relative orientation of the rotatable linear polarizer with respect to the stationary retarder: $\vec{e}_x + \vec{e}_y \to \vec{e}_R$ and $\vec{e}_x - \vec{e}_y \to \vec{e}_L$. After that the circularly polarized light passes through a four-bounce axicon retarder (Fig. 1 of the manuscript), which is made of undoped silicon that is transparent below 500 cm^{-1}. The low-frequency limit is determined by the THz source and the axicon cross section. The sign of the output vortex beams $\vec{e}_{\pm 1}$ is determined by the circular polarization at the axicon input: $\vec{e}_L \to \vec{e}_{+1}$ and $\vec{e}_R \to \vec{e}_{-1}$. The polarization conversion occurs due to phase changes during the four internal reflections inside the axicon. Light propagation in this setup has been analyzed using the ZEMAX software and the expected vorticity of the beam has been confirmed. A photo of the axicon retarder is shown in Fig. S1.

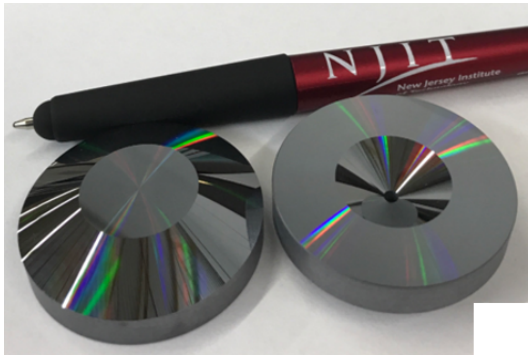

FIG. S1. A photo of the double axicon.

References

[1] F. Sayetat, J. X. Boucherle, and F. Tcheou, Magnetic structures and magnetoelastic phenomena observed in $Tb_3Ga_xFe_{5-x}O_{12}$ garnets, J. Magn. Magn. Mater. **46**, 219 (1984).

[2] R. Hock, H. Fuess, T. Vogt, and M. Bonnet, Crystallographic distortion and magnetic structure of terbium iron garnet at low temperatures, J. of Solid State Chem. **84**, 39 (1990).

[3] M. Lahoubi, M. Guillot, A. Marchand, F. Tcheou, and E. Roudaut, Double umbrella structure in terbium iron garnet, IEEE Trans. Magn. **20**, 1518 (1984).

[4] T. D. Kang, E. C. Standard, P. D. Rogers, K. H. Ahn, and A. A. Sirenko, A. Dubroka, C. Bernhard, S. Park, Y. J. Choi, and S.-W. Cheong, Far-infrared spectra of the magnetic exchange resonances and optical phonons and their connection to magnetic and dielectric properties of $Dy_3Fe_5O_{12}$ garnet, Phys. Rev. B **86**, 144112 (2012).

[5] P. D. Rogers, Y. J. Choi, E. C. Standard, T. D. Kang, K. H. Ahn, A. Dubroka, P. Marsik, C. Wang, C. Bernhard, S. Park, S.-W. Cheong, M. Kotelyanskii, and A. A. Sirenko, Adjusted oscillator strength matching for hybrid magnetic and electric excitations in $Dy_3Fe_5O_{12}$ garnet, Phys. Rev. B **83**, 174407 (2011).

[6] T. D. Kang, E. Standard, K. H. Ahn, A. A. Sirenko, G. L. Carr, S. Park, Y. J. Choi, M. Ramazanoglu, V. Kiryukhin, and S-W. Cheong, Coupling between magnon and ligand-field excitations in magnetoelectric $Tb_3Fe_5O_{12}$ garnet, Phys. Rev. B **82**, 014414 (2010).

[7] A. J. Sievers, and M. Tinkham, Far Infrared Spectra of Rare-Earth Iron Garnets, Phys. Rev. **129**, 1995 (1963).

[8] J. Kaplan, and C. Kittel, Exchange Frequency Electron Spin Resonance in Ferrites, J. Chem. Phys. **21**, 760 (1953).

[9] M. Tinkham, Low-lying spectrum of rare-Earth iron garnet, Phys. Rev. **124**, 311-320 (1961).

[10] T. N. Stanislavchuk, T. D. Kang, P. D. Rogers, E. C. Standard, R. Basistyy, A. M. Kotelyanskii, G. Nita, T. Zhou, G. L. Carr, M. Kotelyanskii, and A. A. Sirenko, Synchrotron-radiation based far-infrared spectroscopic ellipsometer with a full Muller matrix capability, Rev. Sci. Instr. **84**, 023901 (2013).